Microstimulation in The Brain—Does Microdialysis Influence the Activated Volume of Tissue?

D. Krapohl[1,3,*], S. Loeffler[2,*], A. Moser[2] and U.G.Hofmann[1,**]

[1]Institute for Signalprocessing, University of Luebeck, Germany

[2]Institute for Neurology, University of Luebeck, Germany

[3]Department of Information Technology and Media, Mid Sweden University, Sweden

[*]These authors contributed equally to the presented work.

[**]Corresponding author: Ratzeburger Allee 160, 23538 Lübeck, Germany, hofmann@isip.uni-luebeck.de

Abstract: Deep brain stimulation (DBS) has been established as an effective treatment for Parkinson's disease and other movement disorders. The stimulation is currently administered using tetrode-macroelectrodes that target the subthalamic nucleus (STN). This often leads to side effects which bias the surrounding areas, e.g. the speech centre. Targeting a specific brain region can better be achieved with micro-stimulation electrodes with directed electrical field distribution. Experimental studies showed the effectiveness of microelectrode DBS by comparing neurotransmitter outflow before and after the stimulation. The neurotransmitter outflow in close proximity to the stimulation is hereby measured by means of microdialysis. To establish ideal distances and stimulation strength, the electric potential around the stimulation electrode and microdialysis membrane were modelled using COMSOL Multiphysics.

Keywords: deep brain stimulation, microelectrode, microdialysis, electrode-electrolyte interface, impedance

1 Introduction

Since the 1990's tetrode-macroelectrodes are used for DBS in different brain regions. The beneficial effects of this stimulation on motor- as well as psychomotor disorders have been well established [10, 2]. However, partly severe side effects due to lead misplacement or long term tissue impact are reported [17, 14]. Compared to macroelecrodes, the use of microelectrodes for stimulation would provide significant advantages as limitation of the volume of tissue activated, electrophysiologically facilitated accurate probe placement, less tissue impact and facilitation of closed-loop applications [16]. However, stimulation microelectrodes can only be used clinically when their electrical parameters are within the limitations for safe stimulation. Charge per phase and charge density thresholds of 135 - 400 $^{nC}/_{phase}$ respectively 2.3 - 6.7 $^{\mu C}/_{cm^2}$ with pulse widths of 60 - 200 μs have therefore been determined [7, 12]. Nevertheless, charge thresholds depending on the iso- or anisotropy of the tissue, rheobase current and stimulus waveform have to be exceeded in the targeted volume area [9]. For microelectrode stimulation, impedance properties are even more important than for macroelectrode stimulation. It was reported, that substantially different volumes of tissue activated are generated from high, medium and low impedance electrodes [3, 1]. Electrode impedances originate in the formation of a HELMHOLTZ double layer on the electrode-electrolyte interface. A current flow occurs by electrostatic, frequency dependent charging and discharging of the capacitance. But also non-capacitive faradic reactions as well as electrolytic reactions may occur leading to electron transfer across the electrode-electrolyte interface. The processes at the electrode-electrolyte interface can be modelled using equivalent circuit representations as shown in figure 1. The series resistance R_s represents the resistance due to electrolyte solution and cables. R_{ct}, the charge transfer resistance describes the resistance for electrochemical reactions taking place [11]. Z_{cpa} is the frequency dependent constant phase angle element which comprises real- and imaginary part of the impedance Z.
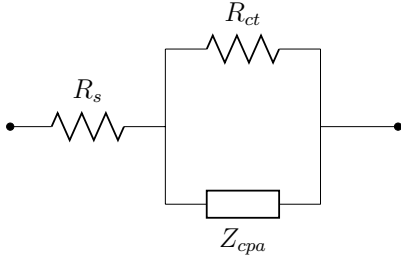
Figure 1: Equivalent circuit representation of the electrode electrolyte interface [6, 13].

Figure 2: Voltage function of a 60 μs 0.5 mA pulse in 0.9 % sodium chloride solution. Represents the voltage function applied as electric potential (V(t)) in the model.

Because of the small size of the microelectrode's geometric surface area (GSA), the charge per unit area at the electrode-electrolyte interface is small. Therefore, high charge-injection capacity, depending on the material, is a prerequisite for microstimulation electrodes [5]. The charge injection capacity Q_{inj} for PtIr alloy has been calculated to be 300 - 350 $\mu C/cm^2$ theoretically, but only about 100 $\mu C/cm^2$ can be injected without causing electrolysis of water [15]. However, disregarding all these parameters, the effectiveness of microelectrode stimulation with cathodic, monopolar, rectangular, 0.5 mA constant current pulses with 60 μs duration and 124 Hz frequency was proven by showing an enhanced outflow of the neurotransmitter γ-aminobutyric acid (GABA) in close proximity to the stimulation microelectrode [8]. Neurotransmitter were sampled with the help of a microdialysis membrane close to the stimulation microelectrode. The influence of the microdialysis membrane as a dielectricum filled with conductive liquid may alter the stimulation properties of the microelectrode as well as the direction and volume in which the electric field is evolving.

2 Measurements

Independent from the modelling approach, voltages, developing under 0.5 mA current stimulation with 60 μs pulse width and electrode impedances were measured. The voltage drop (see figure 2) was measured parallel including cables and connectors using a TDS2004B oscilloscope (*Tektronix Inc., US*) and recorded with NI Signal Express Software (*National Instruments Corp., US*). The signal was downsampled to 200 datapoints using python programming language and later used as a voltage function for COMSOL.
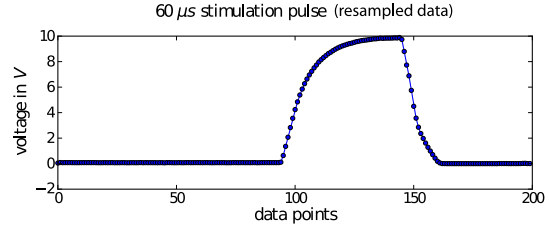
Impedances Z and phase angles *Phi* of two different electrode tip configurations (see figure 6) were measured using a GWINSTEK LCR-821 LCR meter employing the three point measurement method for frequencies ranging from 0.1 to 200 kHz at constant voltage of 0.1 V. Eight measurements were performed with 3 electrodes of two different configurations. Mean value and standard deviation were plotted as Bode Plot representation with double-logarithmic axes for impedances Z and half-logarithmic axes for phase angles *Phi* (see figure 3).
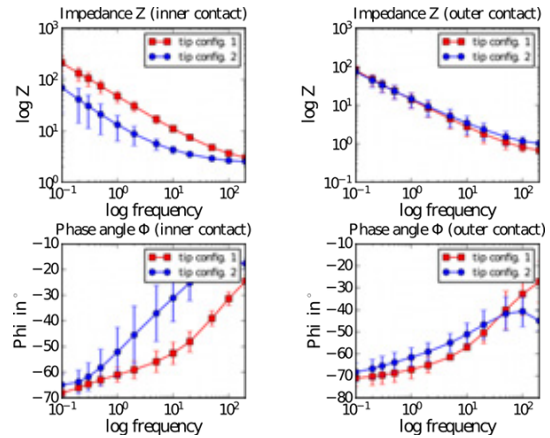

Figure 3: Bode Plot representation of impedances and phase angles for the inner and outer contact area of the concentric, bipolar electrodes and two different electrode tip configurations.

Measures of the realistic arrangement of the CBCBG30 concentric bipolar stimulation microelectrode (*FHC, Maine, US*) and the CMA 11 MD microdialysis probe (*CMA Microdialysis, Sweden*) were taken from a photograph and transfered into a 3D geometric model in COMSOL drawing mode.
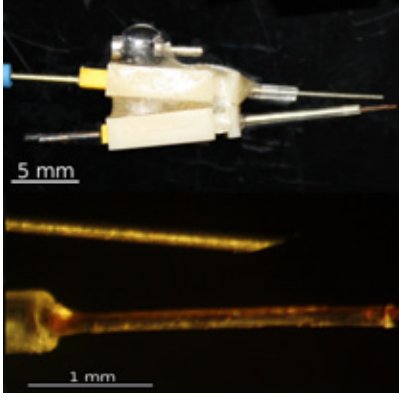
Figure 4: Microdialysis membrane and stimulation electrode fixed in close proximity to a double tube guiding cannula

Material	V $[mm^3]$	A (mm^2)	σ $[S/cm]$
grey matter	166.2725	180.6331	0.00228
Stainless Steel X20CrNi172	0.342189	7.189776	13888.8
CSF	0.907581	7.929236	0.1789
Epoxylite 578EB	0.144513	4.001415	$1e^{-11}$
PtIr 90/10	0.047968	1.333082	$4.081e^6$

Table 1: Volume, area and conductivity of the employed material types for the 5 subdomains modelled.

	Boundary condition	parameter	equation
1	Ground		$V2 = 0$
2	Electric insulation		$n \cdot J = 0$
3	Continuity		$n \cdot (J_1 - J_2) = 0$
4	Electric shielding	$\sigma = 1e^{-11}$, $d = 13e^{-6}$	$n \cdot (J_1 - J_2) = -\nabla_t \sigma d \nabla_t V2$
5	Electric potential	$V_0 =$ V(t)	$V2 = V_0$

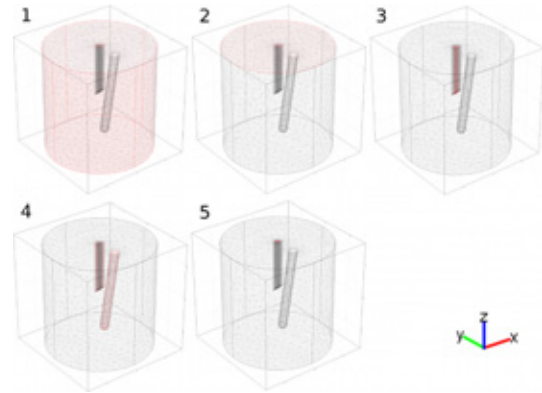Table 2: Exterior and interior boundary conditions assigned to group 1 - 5.

Figure 5: Boundaries group 1 - 5 to which the boundary conditions from table 2 were assigned. Meshing was performed according to the boundaries.

3   Use of COMSOL Multiphysics

COMSOL Multiphysics was used to model the membrane of a microdialysis probe, constantly perfused with KREBS - RINGER bicarbonate buffer pH 7.4, closely resembling the cerebral spinal fluid (CSF), and the tip of a concentric, bipolar stimulation microelectrode with an outer contact made from stainless steel and an inner contact made from PtIr alloy during stimulation with cathodic, monopolar, rectangular, 0.5 mA constant current pulses of 60 μs duration and 124 Hz frequency. COMSOL Electric Currents (AC/DC) module with Conductive Media DC Application Mode solving the generalized partial differential equation for current sources (see equation 1).

$$Q_j = -\nabla \cdot (\sigma \nabla V - J^e) \qquad (1)$$

Isotropic conductivity values were set using the material library for the defined subdomains in the model. For all subdomains, we generally set external current densities, current sources and initial electric potentials to zero and used Lagrange quadratic shape functions for approximation. No infinite elements applied were applied. Table 1 shows the conductivity as well as geometry and description for the subdomains modelled. Five different boundary conditions were assigned to different groups. Table 2 comprises the boundary conditions for groups 1 - 5, shown in figure 5 and their specific properties.

To establish the role of the constant phase angel element Z_{zpa} and the charge transfer resistance R_{ct}, a thin layer of uniform thickness and electrical properties was placed at the electrode - electrolyte interface as explained in [4]. Z_{cpa} was calculated using the factors

$K = 1.57$ m^2/s, β, and the electrode surface area $A = 166.61$ mm^2 with $\omega = 2 \cdot \pi \cdot f$ and $f = 124$ Hz (see equation 2)

$$Z_{cpa} = \frac{K}{A(j\omega)^{-\beta}} \qquad (2)$$

It was assumed that the overpotential η was represented by the voltage difference between the PtIr electrode contact and the surrounding grey matter. Thus, instead of η, the $V(t)$ function was used in the description of the charge transfer resistance R_{ct} as the driving force for faradic reactions to take place (see equation 3 where $R = 8.314472$ $J/K \cdot mole$, $T = 298$ K, $F = 96485.3399$ $C/mole$, $n = 2$ (number of electrons), $I_0 = n \cdot J_0 \cdot A$ (exchange current), $nJ_0 = 6.41 \cdot 10^{-4}$ A/m^2 (normalized equilibrium current density), $A = 166.61$ mm^2 (electrode surface area), $V(t)$ was the overpotential and $\alpha_a = 0.099$ and $\alpha_c = 0.378$ were transfer coefficients).

$$R_{ct} = \frac{V(t)}{I_0 \cdot \left(e^{(\alpha_a \frac{nF}{RT} \cdot V(t))} - e^{(\alpha_c \frac{nF}{RT} \cdot V(t))} \right)} \qquad (3)$$

Meshing was performed according to the boundary conditions. The SPOOLES direct linear systems solver was used with standard settings to solve the model. 91 time steps were calculated according to the time course of the input voltage function $V(t)$. Two different electrode tip configurations were examined (see figure 6). Tip configurations 1 and 2 are bevelled at 45 °. Tip configuration 1 has a inner PtIr contact that is on one level with the outer stainless steel contact and a smooth surface. For tip configuration 2, the inner PtIr contact is raised compared to the outer contact. The tip possesses a rough surface. The electrodes were further modelled having a microdialysis membrane in close promixity, or not. The microdialysis mebrane was modelled as a dielectric material filled with conductive liquid.
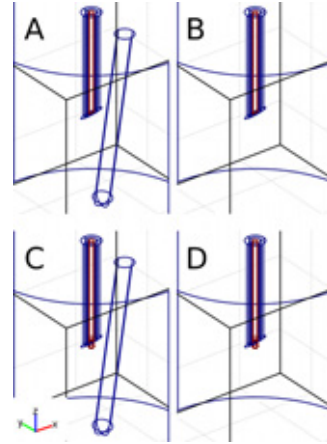

Figure 6: 3D geometry model of the microdialysis membrane and stimulation electrode in close proximity. Two different electrode tip configurations A and B were used in the model.

4 Results

The streamline plot from postprocessing mode in figure 7 shows, qualitatively, that the microdialysis membrane, when included in the model, effects the spread of the electric field from stimulation contact to the outer margins of the tissue volume conductor which were set to ground.
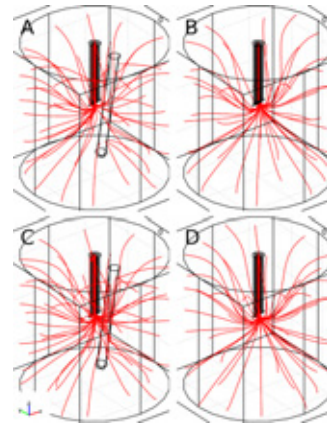

Figure 7: Streamline plots from the different geometric models. A + B: Tip configuration 1 with (A), or without (B) microdialysis membrane. C + D: Tip configuration 2 with (C), or without (D) microdialysis membrane.

For further postprocessing analysis, cross sectional plots for the three dimensions along the x, y and z axis were exported. Figure 8 shows the cross sectional planes in the 3D model.
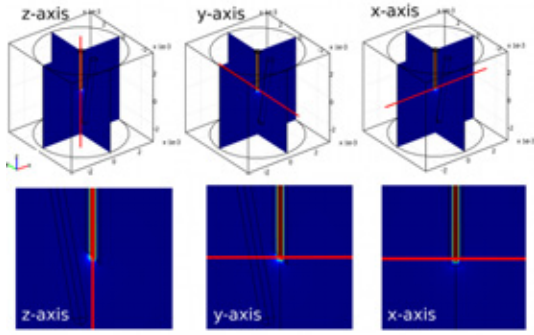
Figure 8: Cross sectional planes x, y and z for which postprocessing analysis was performed.

Figure 9 shows the electric potential for the cross section plots in z-direction including different time steps of the stimulation voltage function. The electric potential in z direction was plottet against the logarithmic distance z. The drop of electric potential from the electrode surface in z-direction was compared between the two different tip configurations (C + D). Further, it was compared whether the presence of the microdialysis membrane affects the voltage drop in z-direction (A+B). Figure 9 shows that the voltage drop for tip configuration 1 is steeper than for tip configuration 2. The presence of the microdialysis membrane does not affect the voltage drop in z-direction.
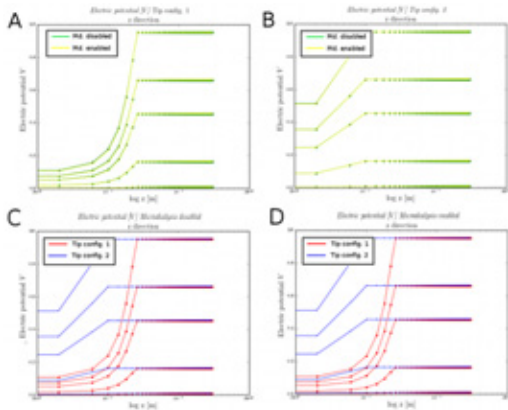

Figure 9: Electric potentials in V for Tip configurations 1 and 2 as well as the electric potential for the enabled or disabled microdialysis membrane.

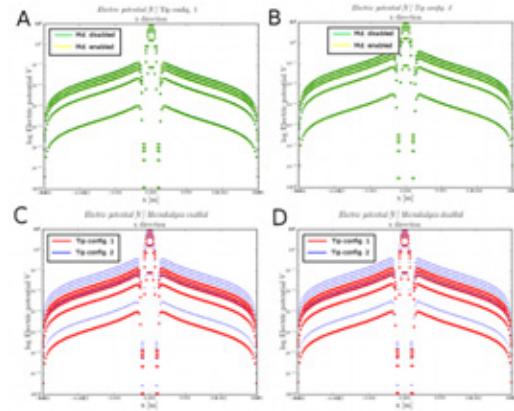Figure 10 demonstrates the voltage drop along the x-axis.

Figure 10: Electric potential in x-direction.

These results show, that the microdialysis membrane in x direction, too, has no effect on the electric potential drop. Again, there is a notable difference between the two electrode tip configurations. The voltage peak at $x = 0$ represents the electric potential on the stimulation contact. The potential drops rapidly on both sides of the stimulation site due to the epoxy insulation material. Then, from the outer contact of the electrode, the potential drops almost linearly along the distance through the tissue. The y-direction is the axis which leads through the contact and the microdialysis membrane. Figure 11 shows the voltage drop of the electric potential in y-direction.
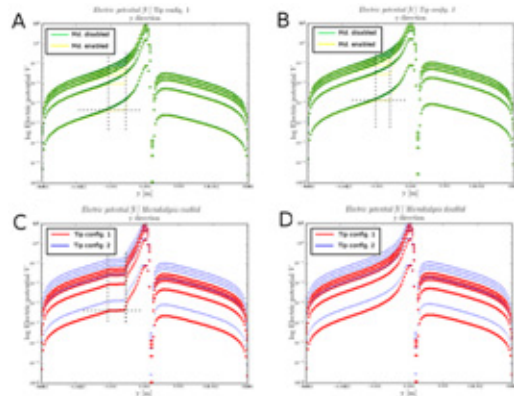

Figure 11: Electric potential in y-direction.

The effect of the microdialysis membrane is clearly visible on this axis. The electrode tips are bevelled. Therefore the voltage drop is non-symmetric in y-direction. The voltage drop on the positive y-axis almost resembles the situation for the x-direction. On the negative y-axis, the steepness of the slope is clearly diminished

on the electrode-tissue boundary. The slope of the voltage drop is zeros from $-0.5mm$ to $-1.0mm$. This occurs co-localized with the microdialysis membrane localization.

5 Discussion

The results of the presented model indicate, that the modification of even minimal tip configurations can lead to strong influences on the electric field distribution in the case of microelectrodes. Further, it is to assume that the microdialysis membrane, indeed has an effect on the spread of the electric potential through the tissue. This effect does, however, not affect the general stimulation behaviour of the microelectrode. Thus, the model of the co-localized microdialysis and microstimulation can be compared with other microstimulation techniques. Our model is based on assumptions which were introduced to reduce the complexity of the electrode-electrolyte interface. Therefore, predictions of current densities are error prone in this state of the model and are not discussed here. It can, however, be observed, that the current density drops rapidly on the electrode-electrolyte interface. That may be an explanation for the comparatively minor damage to the stimulated tissue, which is observed with microstimulation. Further models should emphasize the role of Z_{zpa} R_{ct} and their dependency on the overpotential more thoroughly. The monopolar stimulation, which is now carried out in the model, should be replaced by a bipolar stimulation, which is mostly used for electrical stimulation of cerebral tissue.

References

[1] Mattias Astroem, Ludvig U. Zrinzo, Stephen Tisch, Elina Tripoliti, Marwan I. Hariz, and Karin Wardell, *Method for patient-specic finite element modeling and simulation of deep brain stimulation*, Simulation **47** (2009), 21–28. 1

[2] Alim Louis Benabid, Stephan Chabardes, John Mitrofanis, and Pierre Pollak, *Deep brain stimulation of the subthalamic nucleus for the treatment of parkinson's disease.*, Lancet Neurol **8** (2009), 67–81. 1

[3] Christopher R Butson, Christopher B Maks, and Cameron C McIntyre, *Sources and effects of electrode impedance during deep brain stimulation.*, Clinical neurophysiology : official journal of the International Federation of Clinical Neurophysiology **117** (2006), 447–54. 1

[4] Donald R Cantrell, Samsoon Inayat, Allen Taflove, Rodney S Ruoff, and John B Troy, *Incorporation of the electrode-electrolyte interface into finite-element models of metal microelectrodes.*, Journal of neural engineering **5** (2008), 54–67. 3

[5] Stuart F Cogan, *Neural stimulation and recording electrodes.*, Annual review of biomedical engineering **10** (2008), 275–309. 1

[6] Wendy Franks, Iwan Schenker, Patrik Schmutz, and Andreas Hierlemann, *Impedance characterization and modeling of electrodes for biomedical applications*, IEEE Transactions on Biomedical Engineering **52** (2005), 1295–1302. 1

[7] Jasmine M Henderson, Malcolm Pell, Dudley J O'Sullivan, Elizabeth A McCusker, Victor S C Fung, Philippa Hedges, and Glenda M Halliday, *Postmortem analysis of bilateral subthalamic electrode implants in parkinson's disease.*, Movement disorders : official journal of the Movement Disorder Society **17** (2002), 133–7. 1

[8] A Hiller, Susanne Loeffler, Kristin Haupt, Marek Litza, Ulrich G. Hofmann, and Andreas Moser, *Electrical high frequency stimulation of the caudate nucleus induces local gaba outflow in freely moving rats.*, J Neurosci Methods **159** (2007), 286–290. 1

[9] Alexis M Kuncel and Warren M Grill, *Selection of stimulus parameters for deep brain stimulation.*, Clinical neurophysiology : official journal of the International Federation of Clinical Neurophysiology **115** (2004), 2431–41. 1

[10] Paul Sloan Larson, *Deep brain stimulation for psychiatric disorders.*, Neurotherapeutics **5** (2008), 50–58. 1

[11] E T Mc Adams, A Lackermeier, J A Mc Laughlin, and D Macken, *The linear and non-linear electrical properties of the electrode-electrolyte interface*, Biosensors and Bioelectronics **10** (1995), 67–74. 1

[12] William M. Reichert (ed.), *Indwelling neural implants - strategies for contending with the in vivo environment*, 10 ed., CRC Pupress, Taylor and Francis Gro, Boca Raton, 2008. 1

[13] a Richardot and E T McAdams, *Harmonic analysis of low-frequency bioelectrode behavior.*, IEEE transactions on medical imaging **21** (2002), 604–12. 1

[14] R Mark Richardson, Jill L Ostrem, and Philip A Starr, *Surgical repositioning of misplaced subthalamic electrodes in parkinson's disease: Location of effective and ineffective leads.*, Stereotactic and functional neurosurgery **87** (2009), 297–303. 1

[15] T L Rose and L S Robblee, *Electrical stimulation with pt electrodes. viii. electrochemically safe charge injection limits with 0.2 ms pulses.*, IEEE transactions on bio-medical engineering **37** (1990), 1118–20. 1

[16] Steve Yaeli, Einat Binyamin, and Shy Shoham, *Form-function relations in cone-tipped stimulating microelectrodes*, Frontiers in Neuroengineering **2** (2009), 8. 1

[17] Laura B Zahodne, Michael S Okun, Kelly D Foote, Hubert H Fernandez, Ramon L Rodriguez, Lindsey Kirsch-Darrow, and Dawn Bowers, *Cognitive declines one year after unilateral deep brain stimulation surgery in parkinson's disease: a controlled study using reliable change.*, The Clinical neuropsychologist **23** (2009), 385–405. 1